NASA CR 179584

IN-74
174658
508

NASA

ARC-DRIVEN RAIL ACCELERATOR RESEARCH

PREPARED FOR
LEWIS RESEARCH CENTER
NATIONAL AERONAUTICS AND SPACE ADMINISTRATION
GRANT NAG3-76

FINAL REPORT
February, 1987

Pradosh K. Ray
Mechanical Engineering Department
Tuskegee University
Tuskegee, Alabama

TABLE OF CONTENTS

LIST OF FIGURES

LIST OF TABLES

NOMENCLATURE

A_s = Surface area of the plasma

B = Induced magnetic field

C_f = Friction coefficient

d = Width of the rails

e = Charge of an electron

E = Total energy supplied by the inductor

E_f = Energy lost in plasma by viscous dissipation

E_i = Energy stored in the magnetic field of the rails

E_k = Kinetic energy of the projectile

E_r = Resistive energy loss (total)

F = Force on the projectile

f_1 = Correction factor for the magnetic field

h = Height of the rails

I = Current

I_o = Current in the gun at the beginning of acceleration

j = Current per unit height of the rail

J = Current density

k = Boltzmann's constant

ℓ = Length of the plasma

L_o = Inductance of storage inductor

L' = Inductance gradient of the rails

M = Mass of the projectile

m_e = Mass of electron

m_n = Mass of neutral atom

m_a = Mass of plasma

n = Electron density

n_n = Neutral atom density

P = Pressure

$\bar{P}$ = Average pressure

R_o = Resistance of the storage inductor

R_p = Plasma resistance

R' = Resistance per unit length of the pair of rails

t = Time

t_f = Time of exit of the projectile from the muzzle

$\bar{T}$ = Average temperature

v = Plasma and projectile velocity

v_f = Velocity of the projective at exit from the muzzle

V_a = Muzzle voltage

V_i = Ionization potential

w = Rail separation

x = Position along the x-direction

α = Ablation coefficient

α_o = Average degree of ionization

δ = Skin depth

δ_o = Radius of neutral atom

σ = Conductivity of the rails

σ_o = Conductivity of the plasma

σ_s = Stefan-Boltzmann constant

ρ_a = Average density

μ = Magnetic permeability

μ_r = Magnetic permeability of the rails

ν_{ei} = Electron-ion collision frequency

ν_{en} = Electron atom collision frequency

ν_{eT} = Electron collision frequency, total

$\wedge$ = Coulomb cutoff parameter

RAIL ACCELERATOR PERFORMANCE AND PLASMA CHARACTERISTICS

DUE TO WALL ABLATION

INTRODUCTION

Arc-driven rail accelerators can be used for low thrust orbit transfer of spacecrafts as well as direct earth-to-space launch of payloads [1,2]. These devices also have potential applications in the areas of equation-of-state measurements [3] and impact fusion [4]. A rail accelerator consists of a pair of conductors separated by a distance and connected by a metallic fuse. Walls on the other two sides of the accelerator are made of dielectric materials. The fuse is evaporated by discharging a large current (hundreds of kiloamperes) through it to produce a plasma driving armature.

The current flowing in the rails induces a magnetic field which interacts with the arc current producing the Lorentz force on the arc. If a projectile made of dielectric materials is placed ahead of the arc, the projectile will accelerate along with the arc leading to a very high velocity (several kilometers per second) in a time period of 1-2 ms.

In a rail accelerator, the final velocity of the projectile is theoretically given by

$$v_f = \frac{L'}{2M} \int_o^{t_f} I^2(t)dt \qquad (1)$$

However, rail accelerator experiments have yielded consistently lower projectile velocities than are to be expected from eqn. 1. The loss of performance has been accounted for in the theoretical

1

calculations by using an effective value of the rail inductance gradient or by using empirical friction losses [5,6]. Although empirical friction loss models predict the data reasonably well, they do not provide any physical basis for calculating these losses.

Recently it has been suggested that the reduced acceleration observed in rail accelerator experiments can be explained on the basis of (a) continuous addition of mass to the plasma due to wall ablation and (b) viscous drag in the plasma at high speeds [7,8]. However, there is some uncertainty as to how much ablated material is added to the plasma and its effect on the plasma properties. In this report, these aspects of the rail accelerator problem are investigated with respect to the experiment of Bauer et al. which suffered serious performance losses [9].

EXPERIMENT OF BAUER ET AL. [9]

The space transportation missions using rail accelerators generally require velocities greater than 10 km/s. In 1981, NASA Lewis Research Center sponsored experiments to explore the performance of a single-stage rail accelerator designed to achieve velocities exceeding 10 km/s. In these experiments, a 3-m long, 3.8- by 6.3-mm bore acclerator was tested using a 374-kJ capacitor bank at the Lawrence Livermore National Laboratory.

The rails of the accelerator were made of 6.3 mm square copper bars. Glass reinforced epoxy (G-10) plates formed the side walls and also held the copper bars in place. The projectile was a rectangular parallelopiped (6.3 mm x 3.8 mm x 6.3 mm) made of

polycarbonate and had a mass of 0.2 g. A copper foil placed at the rear of the projectile was used to form the plasma driving armature.

Peak currents of 135 kA were discharged in the accelerator after passing it through a 13 μH pulse shaping inductor. The projectiles were observed to accelerate to a velocity of 2 km/s in the first 0.4 m of the launcher when the acceleration of the projectile ceased. The reasons for the loss of acceleration were not understood at the time and are the subjects of this study.

RAIL ACCELERATOR PERFORMANCE

A. Plasma and Projectile Motion

The motion of the plasma and the projectile is described by

$$\frac{d}{dt}\{(M + m_a)v\} = \frac{L'I^2}{2} - bv^2 \tag{2}$$

$$\text{where } b = C_f\frac{\rho_a A_s}{2}. \tag{3}$$

The acceleration of the plasma and the projectile together is indicated by the term on the left hand side of eqn. 2. The first term on the right hand side of eqn. 2 represents the Lorentz force whereas the second term represents the drag force on the plasma. Expanding eqn. 2, one obtains

$$(M + m_a)\frac{dv}{dt} + v\frac{dm_a}{dt} = \frac{L'I^2}{2} - bv^2 \tag{4}$$

The rate of increase of the mass of the plasma is assumed to be proportional to the power dissipated in the plasma. The constant

of proportionality is the ablation coefficient, α, and it is
defined as [7]

$$\frac{dm_a}{dt} = \alpha \ I \ V_a \tag{5}$$

The constant α is approximately equal to the ratio of the mass of
one atom and the energy required to take the atom from the solid
state through vaporization to ionization. Table 1 lists
calculated values of α for some materials [7].

Table 1
Calculated Value of the Ablation Constant

Material	Ablation Constant
Copper	47 g/MJ
Alumina	13 g/MJ
Polytheylene	4 g/MJ

B. Circuit Equation

The lumped parameter electric circuit of an inductor-driven
rail accelerator is shown in Fig. 1. By applying Kirchoff's law,
the differential equation governing the circuit behavior is
obtained as

$$\frac{d}{dt} \{(L_o + L'x)I\} + (R_o + R'x + R_p)I = 0 \tag{6}$$

The skin effect confines the current to a thin sheet on the rail
surface during the initial part of the acceleration. By assuming a
step-current diffusing into a conductor, the skin depth can be
represented by [10]

REPRESENTS
BACK EMF

PLASMA

RAILS

$L'v$

R_P

$L'X$

$R'X$

$I(t)$

R_O

L_O

+

STORAGE INDUCTOR
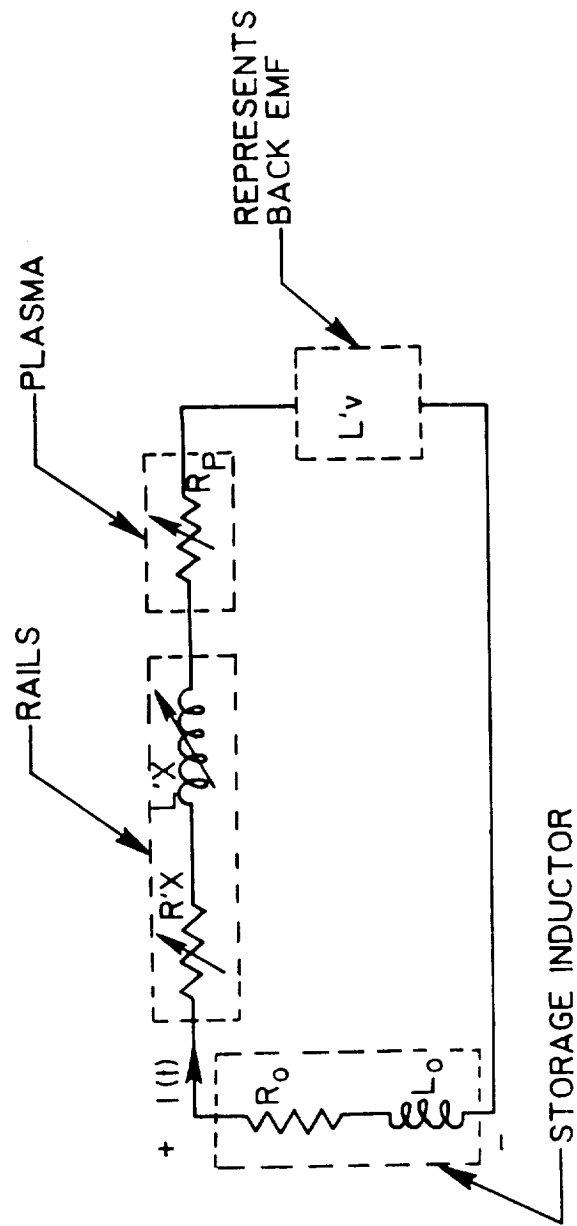
Fig. 1. Equivalent lumped-parametric electric circuit.

$$\delta(t) = \left(\frac{\pi t}{\mu_r \sigma}\right)^{\frac{1}{2}} \tag{7}$$

then,

$$R'(t) = \frac{2}{wD\sigma} \tag{8}$$

where D is equal to the minimum of d or $\delta(t)$.

The muzzle voltage of the accelerator is taken to be the voltage drop across the arc. Hence, the plasma resistance is calculated from

$$R_p(t) = \frac{V_a}{I(t)} \tag{9}$$

Equations 4 to 9 represent a highly coupled nonlinear system. The initial conditions are given by

$$I(0) = I_o$$
$$x(0) = 0 \tag{10}$$

and $v(0) = 0$

C. <u>Energy Partitioning</u>

When the energy stored in the magnetic field of the storage inductor is delivered to the accelerator, it is partitioned in several ways;

a) a part of it is dissipated resistively in the rails, in the plasma and in the resistance of the storage inductor,

b) a part of it is stored in the magnetic field of the rails,

c) a part of it is stored in the form of kinetic energy of the projectile, and

d) a part of it is lost in the viscous dissipation of the plasma.

Their magnitudes are given by

$$E_r = \int_0^{t_f} I^2(t)[R(t)x + R_p(t) + R_o]dt \tag{11}$$

$$E_i = \int_0^{t_f} \frac{L'x}{2} I^2(t)dt \tag{12}$$

$$E_k = \frac{1}{2} Mv^2 \tag{13}$$

$$\text{and} \quad E_f = E - (E_r + E_i + E_k) \tag{14}$$

$$\text{where } E = \frac{L_o}{2} (I_o^2 - I^2) \tag{15}$$

PLASMA CHARACTERISTICS

The plasma properties are evaluated by considering only wall ablation. A complete description of the plasma would require a simultaneous solution of the conservation of mass, momentum and energy equations together with several other related equations so that all the variables are uniquely satisfied. To obtain a physical understanding of the effect of α, the ablation coefficient, on the properties of the plasma, a simplified approach is used here. The plasma is considered to be a rectangular parallelopiped of dimension $1 \times h \times w$ (Fig. 2). The plasma conductivity is taken to be uniform and the plasma is considered to

PLASMA

PROJECTILE

RAILS

X=0

X=ℓ

PLASMA

W

Z

W

h

Y

X

Y
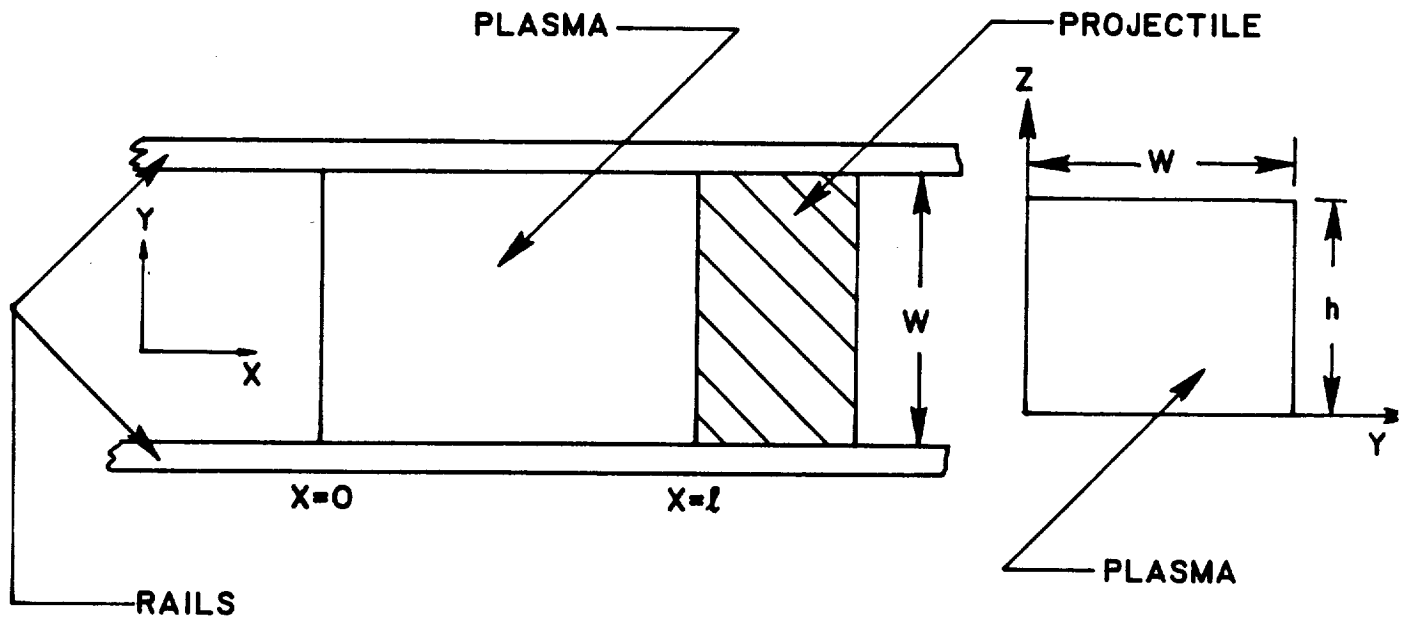
Fig. 2.   Geometry of plasma for modeling.

be singly ionized. It is assumed that at each time step when calculations are performed the plasma is in a quasi-steady state. Furthermore, only the magnetic field and pressure are allowed to vary in the x-direction in the plasma. From the pressure distribution in the plasma, the average pressure is calculated and from this information, the values of other properties are determined. Thus, spatial variations of plasma properties are neglected so that values of plasma temperature, density, etc., are taken as average values.

The current density and the current per unit height of the rail are given by

$$J = \frac{I}{\ell h} \tag{16}$$

$$\text{and} \quad j = \frac{I}{h} \tag{17}$$

Equations 16 and 17 also indicate that

$$J = \frac{j}{\ell} \tag{18}$$

A. Induced Magnetic Field

The magnetic field is given by

$$\frac{dB}{dx} = -\mu J \tag{19}$$

At the leading edge of the plasma, the induced magnetic field is zero. With this condition, eqn. 19 can be integrated to yield

$$B(x) = \mu j (1 - \frac{x}{\ell}) \tag{20}$$

The magnetic field at the trailing edge of the plasma is then given by

$$B(o) = \mu j$$

$$= \frac{\mu I}{h} \tag{21}$$

However, it was found that this expression overestimates the magnetic field and hence, the propulsive force by a factor of 2 or more, as eqn. 21 pertains to rails of infinite height [11]. To estimate the value of the magnetic field more accurately, a correction factor f_1 is introduced here, such that

$$B(x) = f_1 \mu j (1 - \frac{x}{\ell}) \tag{22}$$

The value of f_1 can be found by normalizing the $\underline{J} \times \underline{B}$ force with that calculated from the experimental data at the beginning of acceleration.

B. **Pressure**

It is assumed that the pressure distribution in the plasma can be represented by [12]

$$\rho_a \frac{dv}{dt} + \frac{dP}{dx} = JB \tag{23}$$

To calculate the pressure at the beginning of acceleration, the contribution of the first term in eqn. 23 is neglected. Substituting the values of J and B from equations 18 and 22 into eqn. 23, one obtains

$$\frac{dP}{dx} = \frac{f_1 \mu j^2}{\ell} (1 - \frac{x}{\ell}) \tag{24}$$

For a pure electromagnetic acceleration of the plasma, the pressure at the trailing edge is zero. With this condition, eqn. 24 can be integrated to yield

$$P(x) = \frac{f_1 \mu j^2}{\ell} \left(x - \frac{x^2}{2\ell} \right)$$ (25)

The pressure exerted by the plasma at the base of the projectile is then

$$P(\ell) = \frac{f_1 \mu j^2}{2}$$

$$= \frac{f_1 \mu I^2}{2h^2}$$ (26)

The force on the projectile at the beginning of acceleration can also be represented by

$$F = \frac{L' I^2}{2}$$ (27)

Equating the two forces, one obtains

$$\frac{f_1 \mu I^2}{2h^2} (hw) = \frac{L' I^2}{2}$$ (28)

giving $f_1 = \frac{L' h}{\mu w}$ (29)

In the experiment of Bauer et al., h = 3.85 mm, w = 6.35 mm and L' was measured to have a value of 0.5 μH/m. Substituting these

values of L', h and w into eqn. 29, the value of f_1 is found to be equal to 0.24.

The average pressure can be obtained as

$$\overline{P} = \frac{f_1 \mu j^2}{3} \tag{30}$$

C. **Temperature and Degree of Ionization**

The average temperature of the plasma can be obtained from the average pressure by assuming that the electrons, the ions and the neutral atoms are at the same temperature. Hence, $\overline{P}$ and $\overline{T}$ are related by

$$\overline{P} = nk\overline{T}(1 + \frac{1}{\alpha_o}) \tag{31}$$

where α_o is the average degree of ionization and is defined by

$$\alpha_o = \frac{n}{n + n_n} \tag{32}$$

The degree of ionization can be obtained from the Saha equation [13]

$$\frac{\alpha_o^2}{1 - \alpha_o^2} = \frac{kTK(T)}{\overline{P}}$$

$$= C \tag{33}$$

where $K(T)$ is given by

$$K(T) = 2.41 \times 10^{21} T^{3/2} \exp[\frac{-eV_i}{kT}] \tag{34}$$

Thus,

$$\alpha_o = [\frac{C}{1 + C}]^{1/2} \tag{35}$$

D. Density and Length

Neglecting the mass of the electrons, the average density of the plasma is given by

$$\rho_a = (n + n_n)m_n \tag{36}$$

Substituting the value of α_o from eqn. 32 into eqn. 36, one obtains

$$\rho_a = \frac{nm_n}{\alpha_o} \tag{37}$$

The length of the plasma is calculated from

$$\ell = \frac{m_a}{\rho_a hw} \tag{38}$$

E. Conductivity and Resistance

The plasma conductivity is calculated from [14]

$$\sigma_o = \frac{ne^2}{m_e \nu_{eT}} \tag{39}$$

$$\text{where } \nu_{eT} = \nu_{ei} + \nu_{en} \tag{40}$$

ν_{ei} and ν_{en} are given by [14]

$$\nu_{ei} = 3.62 \times 10^{-6} nT^{-3/2} \ln\Lambda \tag{41}$$

$$\text{and } \nu_{en} = 2.60 \times 10^4 \delta_o^2 n_n T^{1/2} \tag{42}$$

The Coulomb cutoff parameter $\wedge$ is given by [14]

$$\wedge = 1.23 \times 10^7 T^{3/2} n^{-1/2} \tag{43}$$

The resistance of the plasma is given by

$$R_p = \frac{w}{\sigma_o \ell h} \tag{44}$$

F.   Energy Dissipation

The energy dissipated in the plasma by ohmic heating must be balanced by the heat loss from the plasma. Because of the high plasma temperature, the heat loss is primarily by radiation. Thus,

$$V_a I = 2(wh + h\ell + \ell w)\sigma_s T^4 \tag{45}$$

RESULTS AND DISCUSSION

A.   Accelerator Performance

To determine the position of the projectile as a function of time, equations 4 to 9 are solved numerically together with the boundary condition specified in eqn. 10 by using a finite difference approximation with a time interval of 5 μs. The values of α and b are adjusted to provide a good fit to the data. Calculated values of α indicate that it ranges from 4 g/MJ for polyethylene to 47 g/MJ for copper [7]. It was found that values of $\alpha = 10$ g/MJ and b = 7.0 x 10^{-4} kg/m provide a good fit to the data. The values of the parameters used in solving the rail accelerator equations are taken from the experiments of Bauer et al. and listed in Table 2 [9].

Table 2
Input Data for Theoretical Calculations [9]

Parameter	Value
d	6.35 mm
I_o	135 KA
L_o	13 μH
L'	0.50 μH/m
M	0.2 g
V_a	200 volt
R_o	650 μohm
w	6.35 mm
μ_r	$4\pi \times 10^{-7}$ H/m
σ	0.58×10^8 ohm^{-1}-m^{-1}

The position of the projectile computed from these equations as a function of time is shown in Fig. 3 in solid line. For comparison, the data points from the experiment of Bauer et al. [9] are shown in solid circles. The theoretical calculation without ablation and viscous drag is also shown in Fig. 3 in broken lines.

The physical significance of the term b remains somewhat ambiguous. It has been observed that by simply using b as a parameter, one can fit the rail accelerator data from theoretical calculations [6]. Since b is directly related to the size of the bore, its value is expected to vary from one experimental set-up to another. However, using representative values of ρ_a and A_s from the experiments of Bauer et al. and $b = 7.0 \times 10^{-4}$ kg/m, the value of C_f is found from eqn. 3 to be greater than 0.01. This is larger than the representative values of $C_f = 0.0015$ to 0.006 estimated from hypersonic friction measurements [7]. The physical nature of the viscous drag in the boundary layers of an accelerating plasma in a strong magnetic field is poorly understood at present and much more study is needed in this area.

If the viscous drag in the plasma is ignored and only the wall ablation is taken into account, then the data is not well reproduced. Figure 4 shows the position of the projectile against time with α ranging from 7.5 to 50 g/MJ and $b = 0$. The data points of Bauer et al. are shown in solid circles.

The percentage distributions of the energy delivered from the inductor are calculated using equations 11 to 15 and are shown in Fig. 5 as a function of time. Maximum energy is lost in the plasma and most of the losses are in resistive heating.
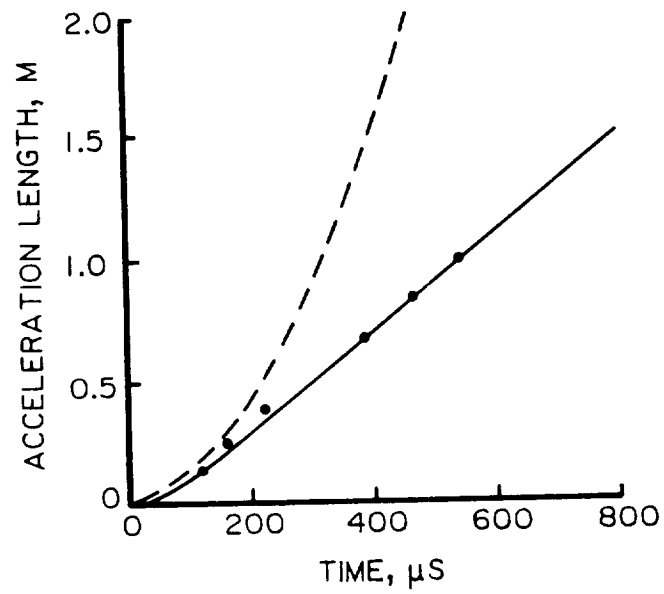
Fig. 3. Acceleration length as a function of time. Solid line represents theoretical calculations from this study. Solid circles are data points from the experiment of Bauer et al. [9]. Broken lines represent calculation without ablation and viscous dissipation in the plasma.
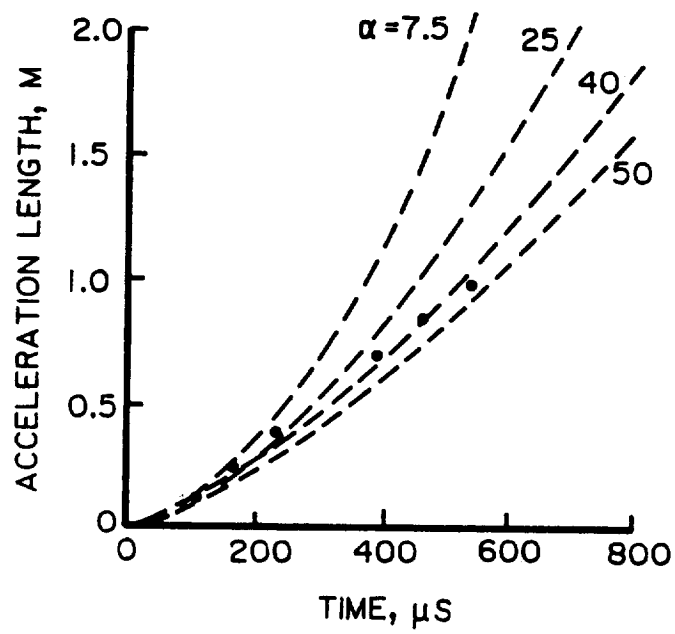
Fig. 4. Acceleration length as a function of time with ablation.
Solid circles represent data points. The unit of α is in
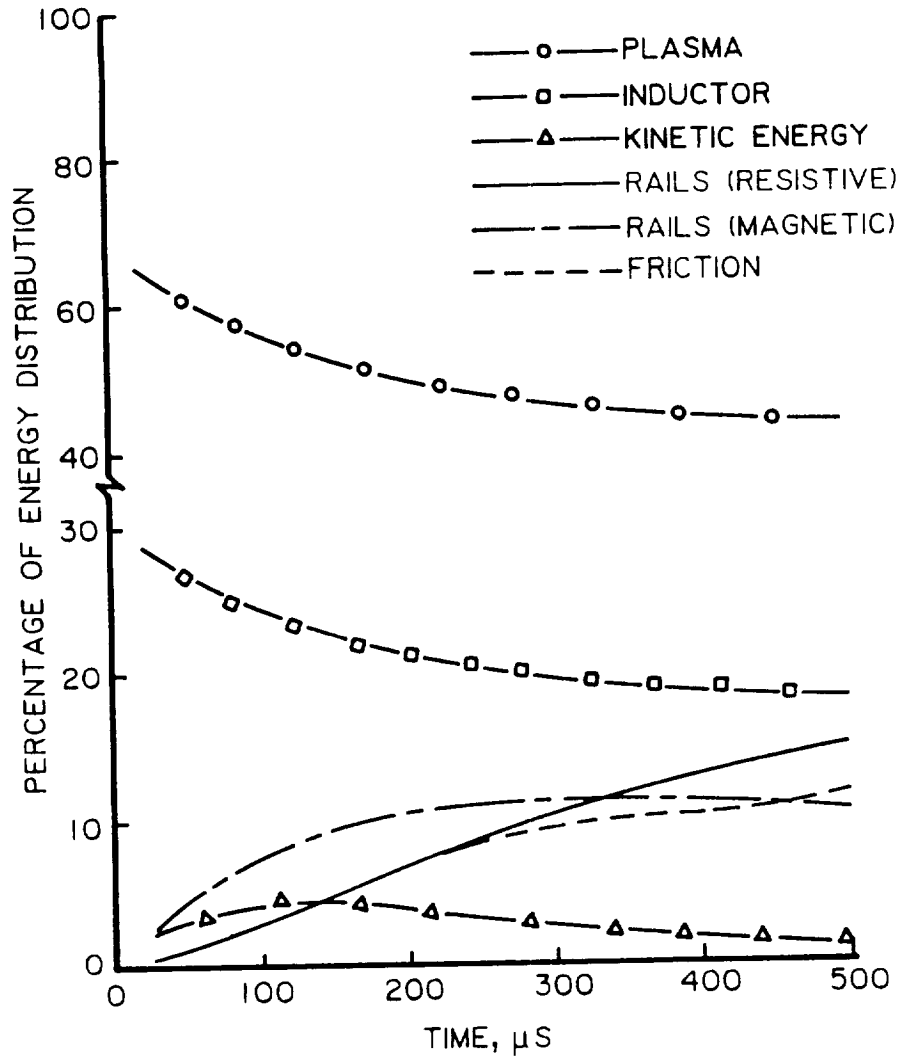g/MJ. The viscous drag is ignored here.

Fig. 5. Percentage of energy distribution as a function of time. These are obtained from theoretical calculations.

B. Plasma Characteristics

To determine the plasma parameters at the beginning of acceleration, a plasma mass is assumed at first. Next, a plasma temperature is assumed and from the average pressure at the beginning of acceleration obtained earlier, the degree of ionization, the plasma length, the plasma resistance and the voltage drop across the plasma are calculated. The calculated voltage drop across the plasma is then checked against the measured muzzle voltage. If the two values are different, a new temperature is selected and the iteration process is continued until the two values do not differ by more than 1 volt. The plasma temperature is then checked against the temperature obtained from eqn. 45. If the two temperatures do differ by more than one percent, then a new plasma mass is selected and the whole process is repeated.

The two temperatures match when the plasma mass is 28 mg. In the experiment of Bauer et al., the mass of the foils was approximately 30 mg. This implies that over 90 percent of the foil was converted into plasma. Table 3 lists several calculated plasma parameters at the beginning of acceleration.

Table 3
Calculated Plasma Parameters at the
Beginning of Acceleration

Parameter	Value
T	$25,600^\circ$ K
α_o	0.68
n	$1.4 \times 10^{26}/m^3$
σ_o	$21,510$ ohm^{-1}m^{-1}
ρ_a	22.1 kg/m^3
ℓ	51.8 mm

For subsequent calculations, values of α = 7.5, 15 and 40 g/MJ are assumed. Next, a plasma length and a plasma pressure are assumed. The plasma temperature is calculated from eqn. 45. From $\bar{P}$, $\bar{T}$ and m_a, a new value of plasma density and length are obtained. The value of plasma length is used to get a new value of $\bar{T}$ whereas the plasma density is used in eqn. 23 to yield a new $\bar{P}$. The iteration process is repeated until the values of temperature, pressure, density and length of the plasma converge.

The temperature, the degree of ionization, the electron density, the conductivity, the density and the length of the plasma are plotted as a function of time in Figs. 6 to 11 up to t = 500 μs. The temperature, the degree of ionization, the electron density and the conductivity of the plasma decrease with time as mass is added to the plasma. Also, at a given time, their values are lower for higher values of α. The density and the length of the plasma increase with time and at a given time increase with α.

Since the plasma length increases at a faster rate than the conductivity decreases, the plasma resistance calculated from eqn. 44 decreases rapidly with time and does not reproduce the muzzle voltage well. Further study is needed in this area, although a simplified model such as this is not expected to provide a complete agreement with observations.

CONCLUSION

The loss of performance in the experiment of Bauer et al. is explained on the basis of wall ablation and viscous drag in the plasma. The temperature, the degree of ionization, the electron
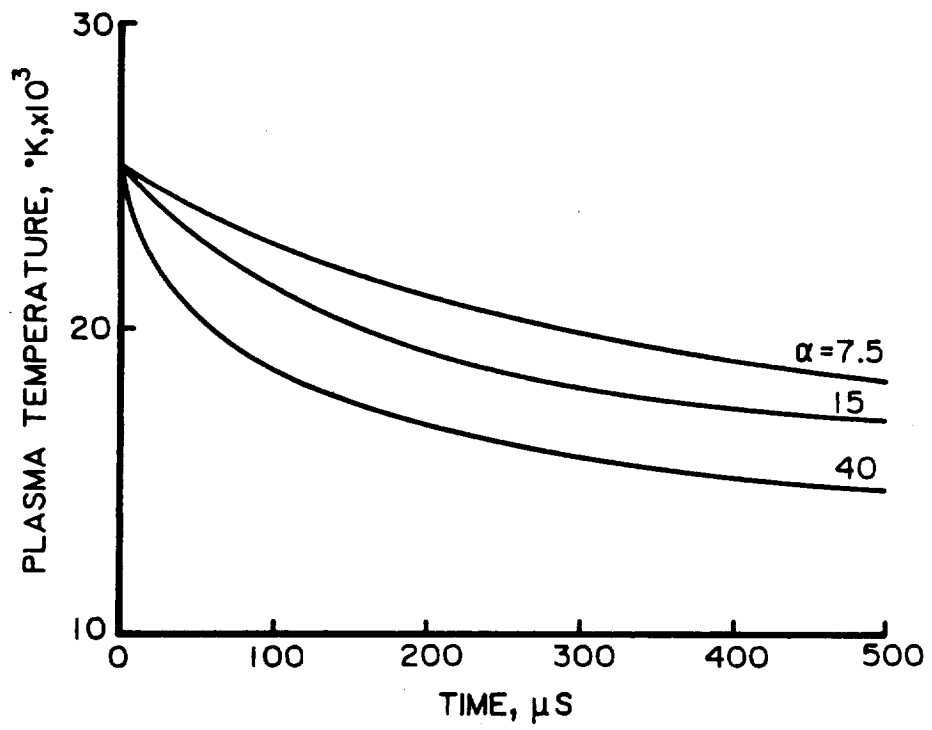
Fig. 6. Plasma temperature versus time with ablation. The unit of α is in g/MJ.
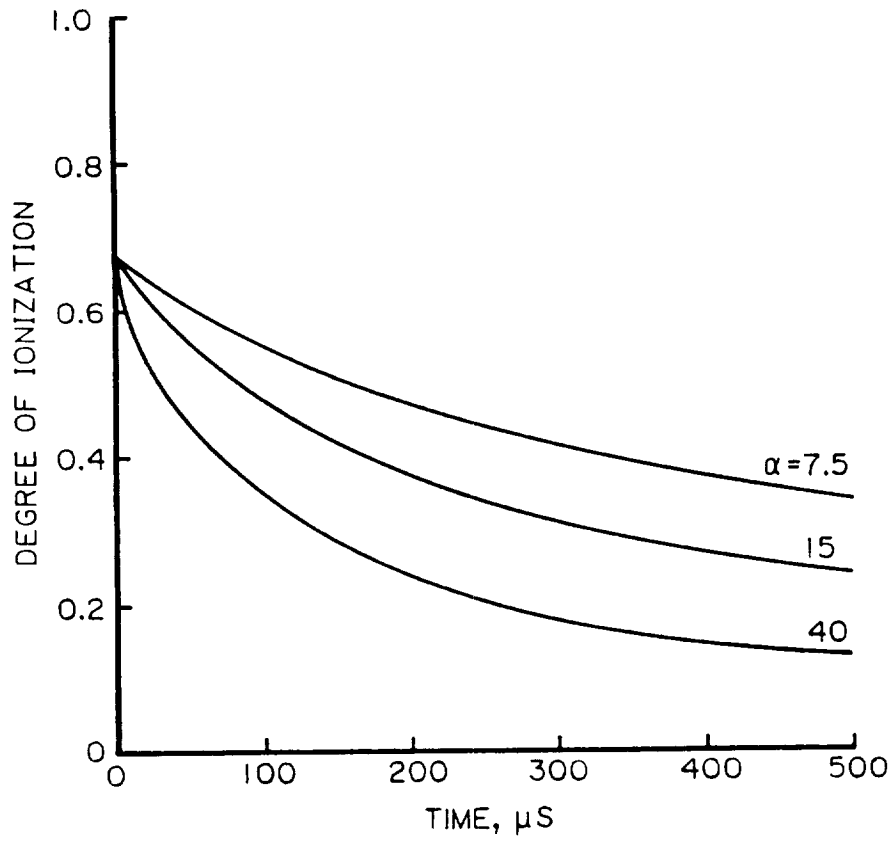
Fig. 7. Degree of ionization versus time with ablation. The unit of α is in g/MJ.
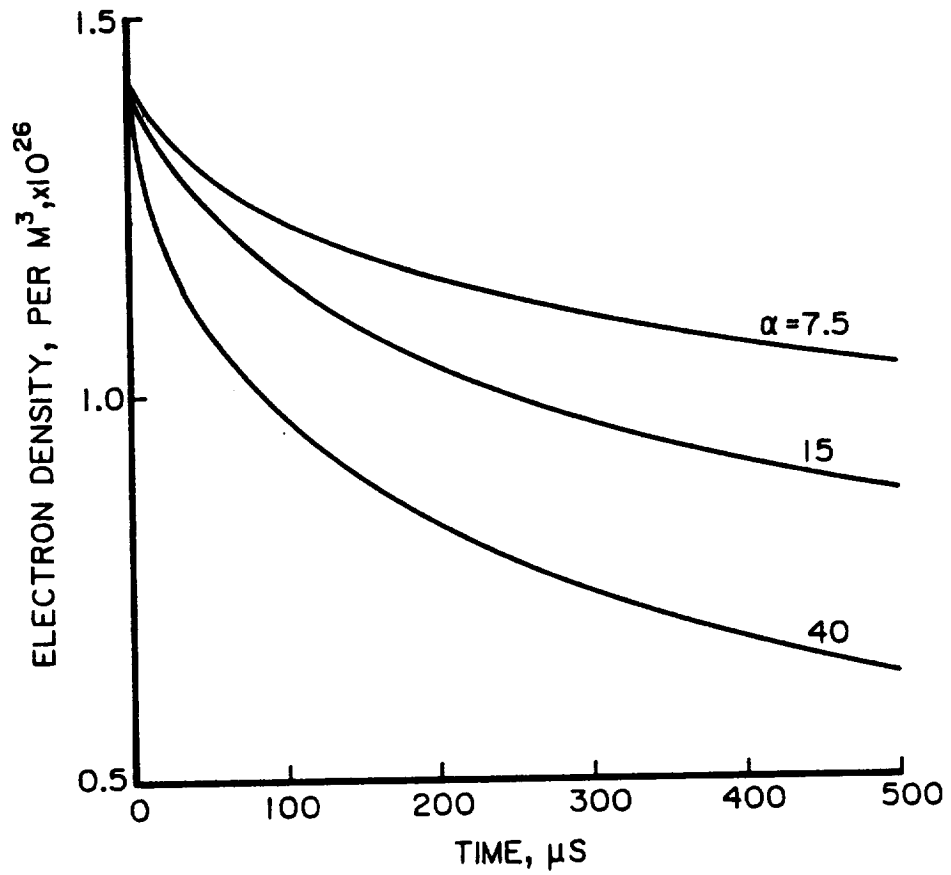
Fig. 8.   Electron density as a function of time with ablation.   The unit of α is in g/MJ.

Fig. 9. Plasma conductivity as a function of time with ablation. The unit of α is in g/MJ.
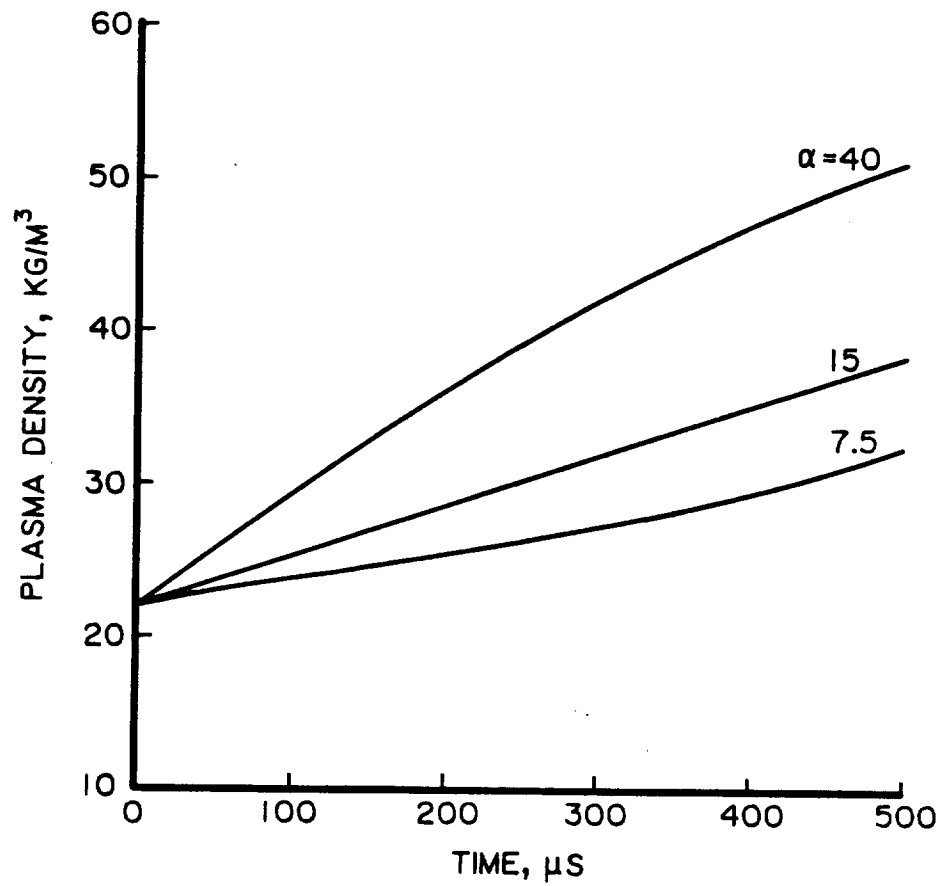
Fig. 10. Plasma density versus time with ablation. The unit of α is in g/MJ.

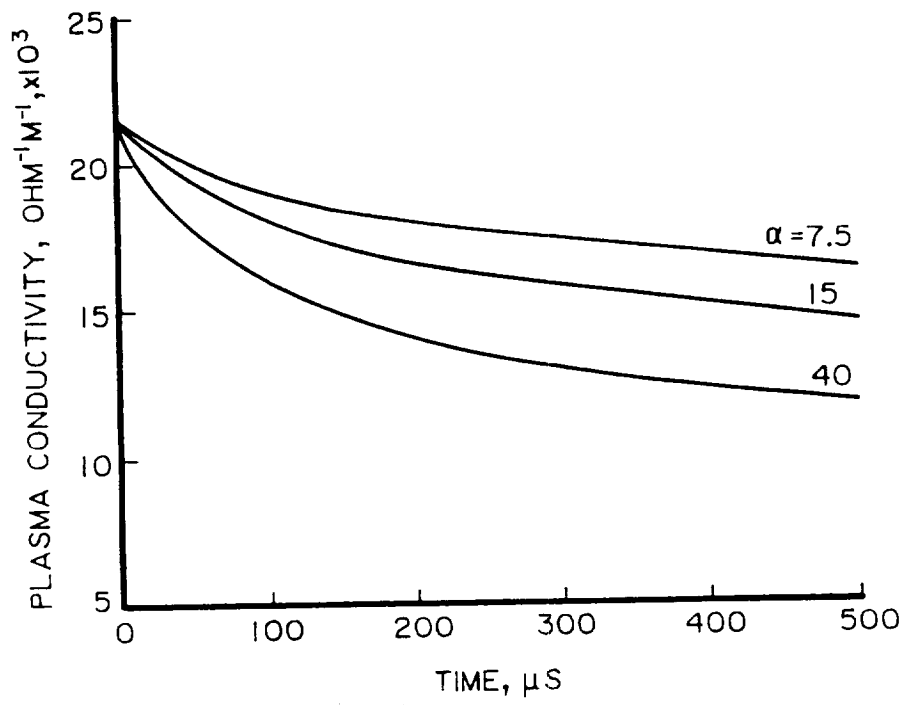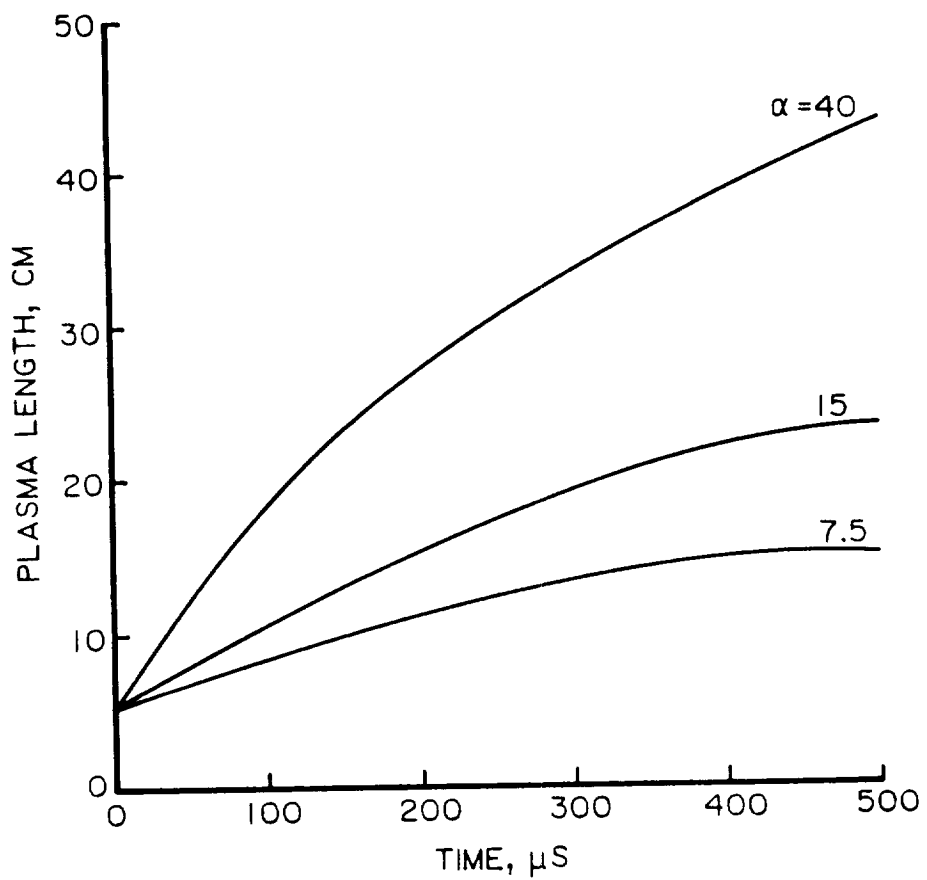Fig. 11. Plasma length versus time with ablation. The unit of α is in g/MJ.

density and the conductivity of the plasma decrease as the ablated

mass is added to the plasma whereas the density and the length of

the plasma increase.

ARC DIAGNOSTICS IN A RAIL ACCELERATOR

INTRODUCTION

Between 1981 and 1984, many rail accelerator tests were
conducted at NASA Lewis Research Center [1,15,16]. Initial tests
were performed on a 3 mm^2 bore accelerator using a 5-kJ capacitor
bank to demonstrate concept and to gain an understanding of the
physics principles. Later tests were done on 1-m-long, 4- by 6-mm
bore (3 different configurations) and 1-m-long, 12.5- by 12.5mm
bore rail accelerators using a 240 kJ capacitor bank. The small
bore accelerators were tested for structural integrity and its
effect on accelerator performance. The medium bore accelerator was
used to understand the physics of plasma armature and its scaling
laws to a larger bore. It had clear polycarbonate sidewalls to
photograph the plasma arc formation and acceleration. The
performance of this accelerator was determined as a function of
current, bore pressure and the amount of plasma blowby.

Plasma blowby occurs when a portion of the arc leaks around
the projectile due to displacements of the rails and the sidewalls
caused by the dynamic stress generated in the accelerator
structure. If sufficient amount of plasma blows by the projectile,
a secondary arc will strike in front of the projectile, thereby
reducing the force available for acceleration. However, the amount
of plasma in a typical blowby is usually too small to be properly
recorded by the magnetic and optical probes. In one of the tests
(Test no. 101), a second aluminum foil was glued in front of the
projectile to deliberately create a secondary arc ahead of the

29

projectile, so that the response of the probes to two simultaneously accelerating arcs can be observed. The results of this test are summarized in this report. The results of other tests using both the small bore and the medium bore accelerators can be found in ref. 1.

EXPERIMENTAL METHODS

The 12.5-mm square bore accelerator was used for this test. The initial energy is stored in two capacitor bank modules which were charged to 7.1 kV. The amount of energy stored in the two modules was 62 kJ. The natural circuit inductance of 1.7 μH maintained delivery of the current to the accelerator after the capacitor banks were crowbarred at the peak of the current pulse. For this test, the accelerator current was 268 kA (fig. 12). A detailed description of the test facility can be found in ref. 17.

The projectile was initially located at a position 30 cm from the breech. The mass of the projectile was 1.69 g. An insulation foil was attached behind the projectile to protect it from direct contact with the arc. A thin aluminum foil was glued to its back to generate the plasma driving armature and another aluminum foil was glued to its front to generate the secondary arc ahead of the projectile.

In the absence of any other conducting path, the current flowing through the rail accelerator circuit must pass through the arc. The total current flowing through the rails and, therefore, the arc was measured by a Pearson current transformer as well as a Rogowski coil. The former was mounted near the header assembly
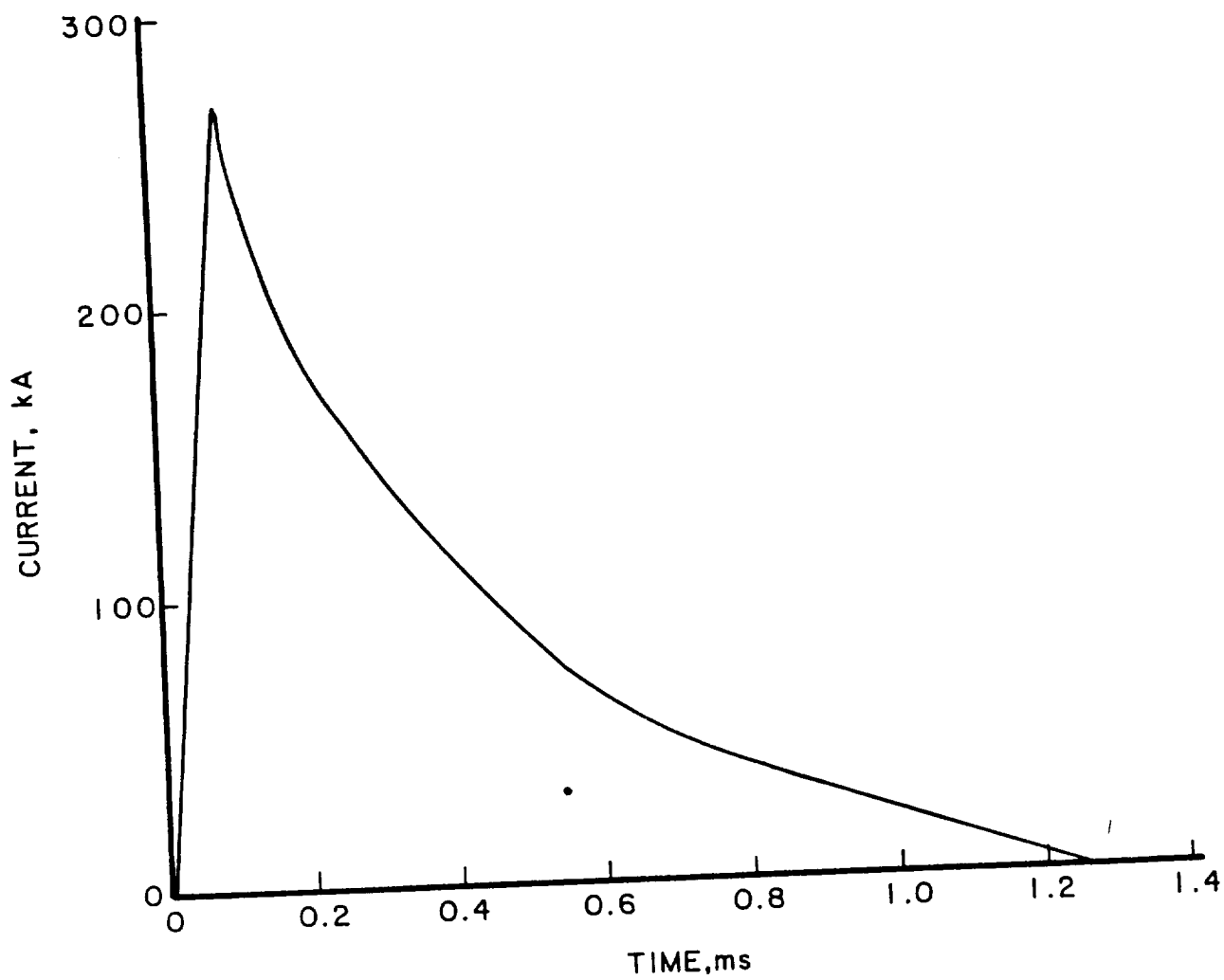
Fig. 12. Current in the accelerator as a function of time.

whereas the latter was positioned near the breech of the accelerator.

The breech and muzzle voltages of the accelerator were measured by resistive divider networks. The breech voltage is essentially the voltage supplied by the inductor. The muzzle voltage represents the voltage drop across the arc and hence is a measure of its conductivity.

The accelerating arc has a finite length. To locate the passing arc, both fiber optic and magnetic probes were stationed at suitable intervals along the length of the accelerator as shown in Fig. 13. The fiber optic probe measures the amount of light falling on it and converts it to a voltage signal. The front edge of such a voltage pulse identifies the leading edge of the arc. The side walls of the accelerator are made of a clear polycarbonate material to permit visual observation of arc acceleration. One end of a fiber optic bundle is embedded in the polycarbonate wall while the other end is connected to a phototransistor.

Each magnetic probe is a coil consisting of five wire turns wound on non-metallic rod. Both 6 mm and 12 mm diameter coils were used. The coils are oriented with their axes parallel to the bore of the accelerator so that they detect primarily the magnetic field associated with the arc current. These $\dot{B}$-loop probes produce a voltage proportional to the time rate of change of the magnetic field. As the arc approaches a $\dot{B}$-loop station, the magnetic flux in the coil increases. When the center of the arc is directly in line with the center of the probe there is no voltage output from the probe. As the arc moves away from the probe, the output

STREAK CAMERA VIEW

POLYCARBONATE
SIDE WALL

RAIL
12.5 x 18.5mm

FIBER OPTIC
PROBE

Ḃ -COIL
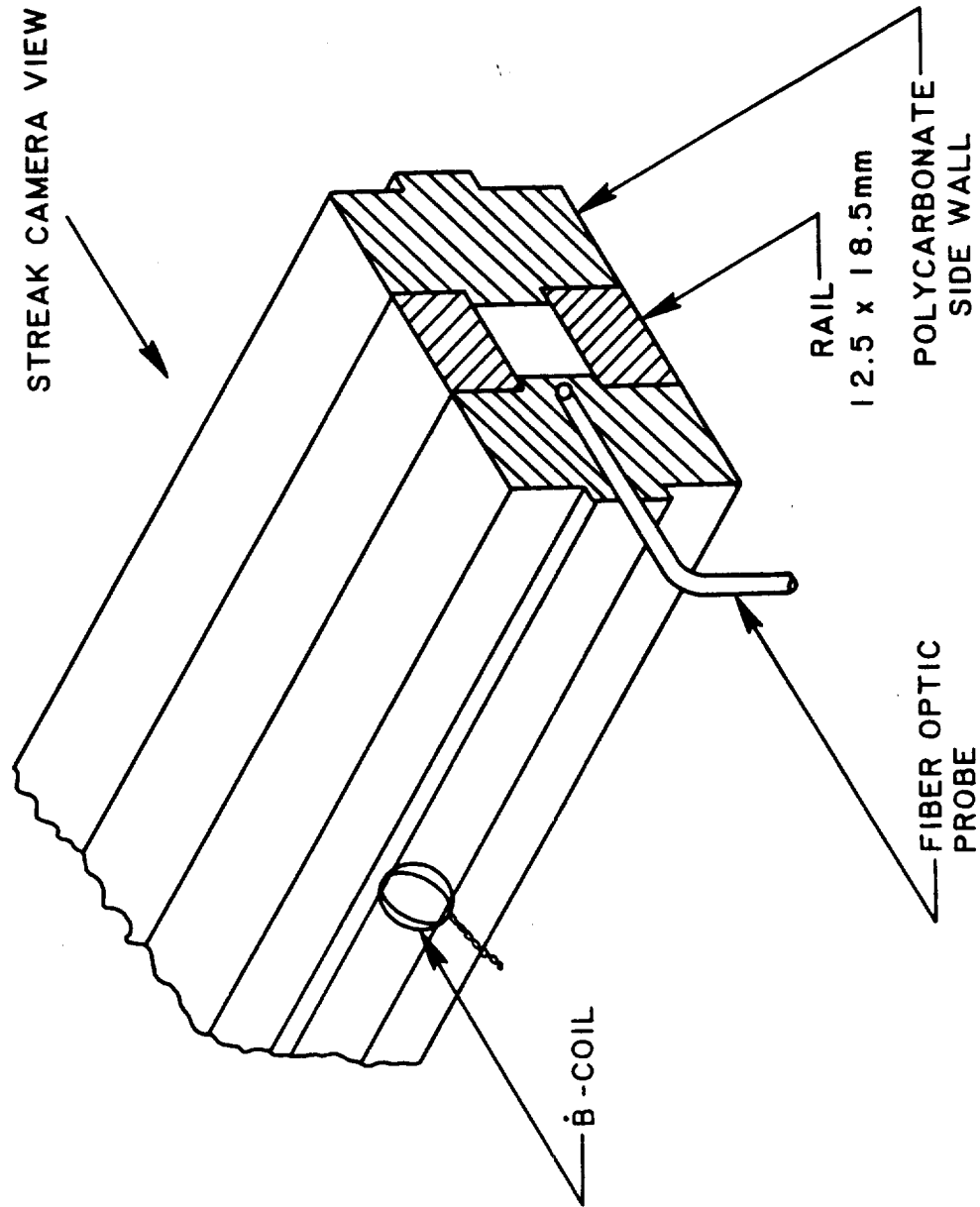
Fig. 13. Accelerator bore with schematic of diagnostic probes.

voltage is of opposite polarity. The wire turns of each successive B-loop stations are wound in opposite directions.

In addition, the visual observation of the arc has been made possible by the use of high speed streak camera photography. These photographs display the time variation of the position of the luminous portion of the arc.

RESULTS AND DISCUSSION

The streak camera photograph reveals in detail the formation of the arcs and their subsequent acceleration in Fig. 14. The front arc being unrestrained, accelerates rapidly. Near the muzzle of the accelerator, this forward arc can be seen to split into two parts.

The rear arc, which is constrained behind the projectile, accelerates at a much slower rate. It too splits into two parts but the separation occurs earlier near the middle of the accelerator. It can be observed from the photograph that the acceleration of the arc occurs only for a short period of time after the discharge is initiated.

The output of the fiber optic bundle located at 70 cm is shown in Fig. 15. The first pulse is from the front arc which has not yet separated. The two other pulses are from the rear arc which has separated at this point.

The output from the B-coil located at 90 cm is shown in Fig. 16. The first two bipolar pulses are from the front arc which by now is separated while the two other bipolar pulses are from the arc behind the projectile.

Fig. 14. Streak camera photograph of arc acceleration.
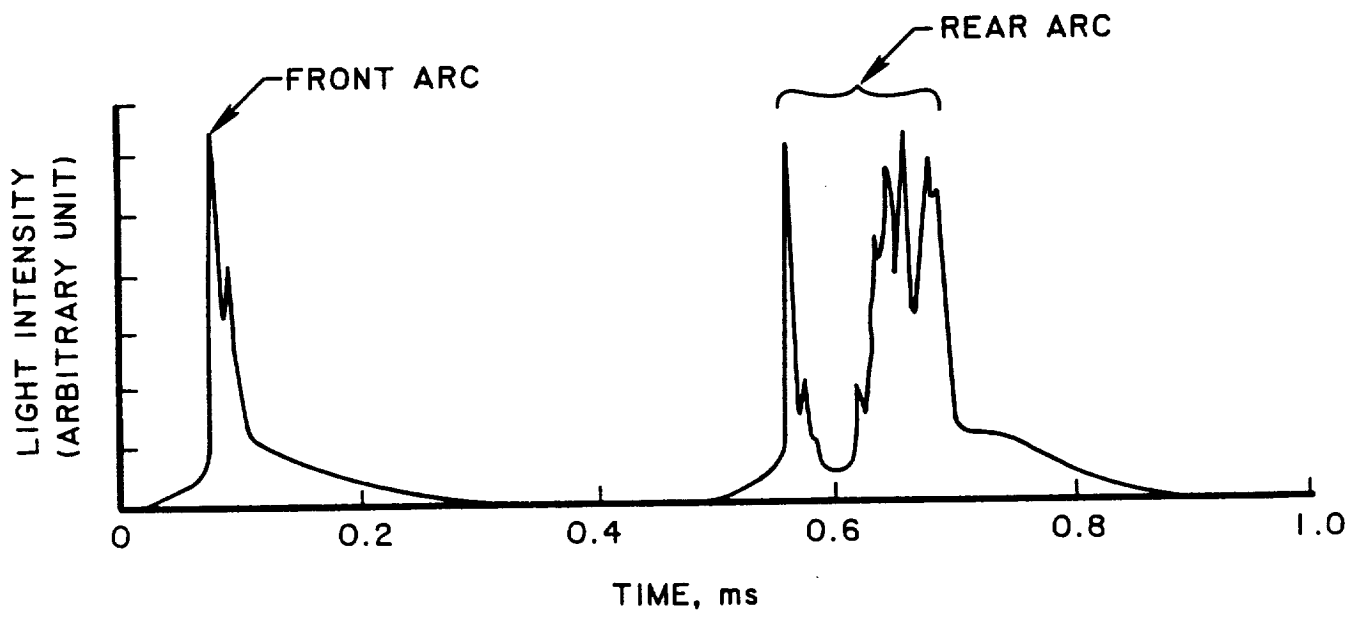
Fig. 15. Output of the fiber optic probe located at 70 cm.
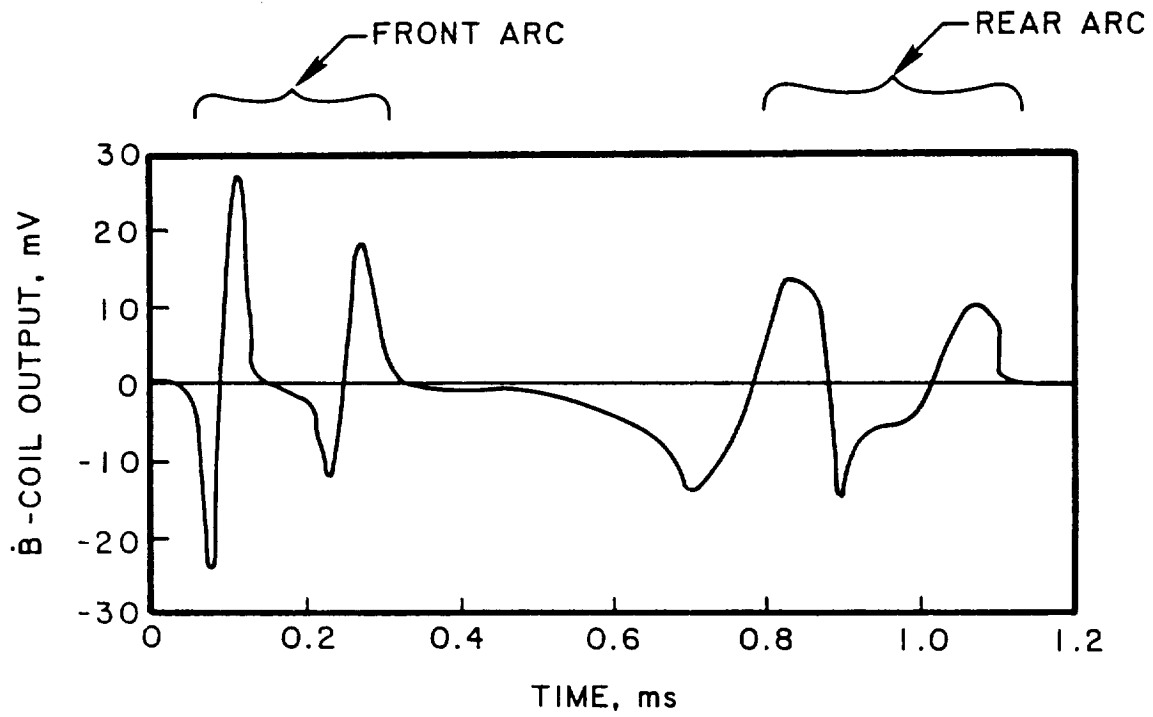
Fig. 16. Output of the Ḃ-coil probe located at 90 cm.

The positions of the arcs as a function of time are plotted in Fig. 17. The data from the streak camera photograph and fiber optic probes refer to the front edge of the arcs whereas the data from the $\dot{B}$-coil probes identify the center position of the arc. The front arc reaches a velocity of 5.4 km/s. The exit velocity of the rear arc and hence, of the projectile is found to be 1.1 km/s.

CONCLUSION

The locations of two accelerating arcs, one in front and the other behind the projectile, were determined as a function of time from streak camera photograph and from optical and magnetic probes. Although the magnetic probes provide more consistent data, the results from all three measurements are in agreement with each other. It is concluded that sufficient amount of blowby plasmas in a rail accelerator can be detected.
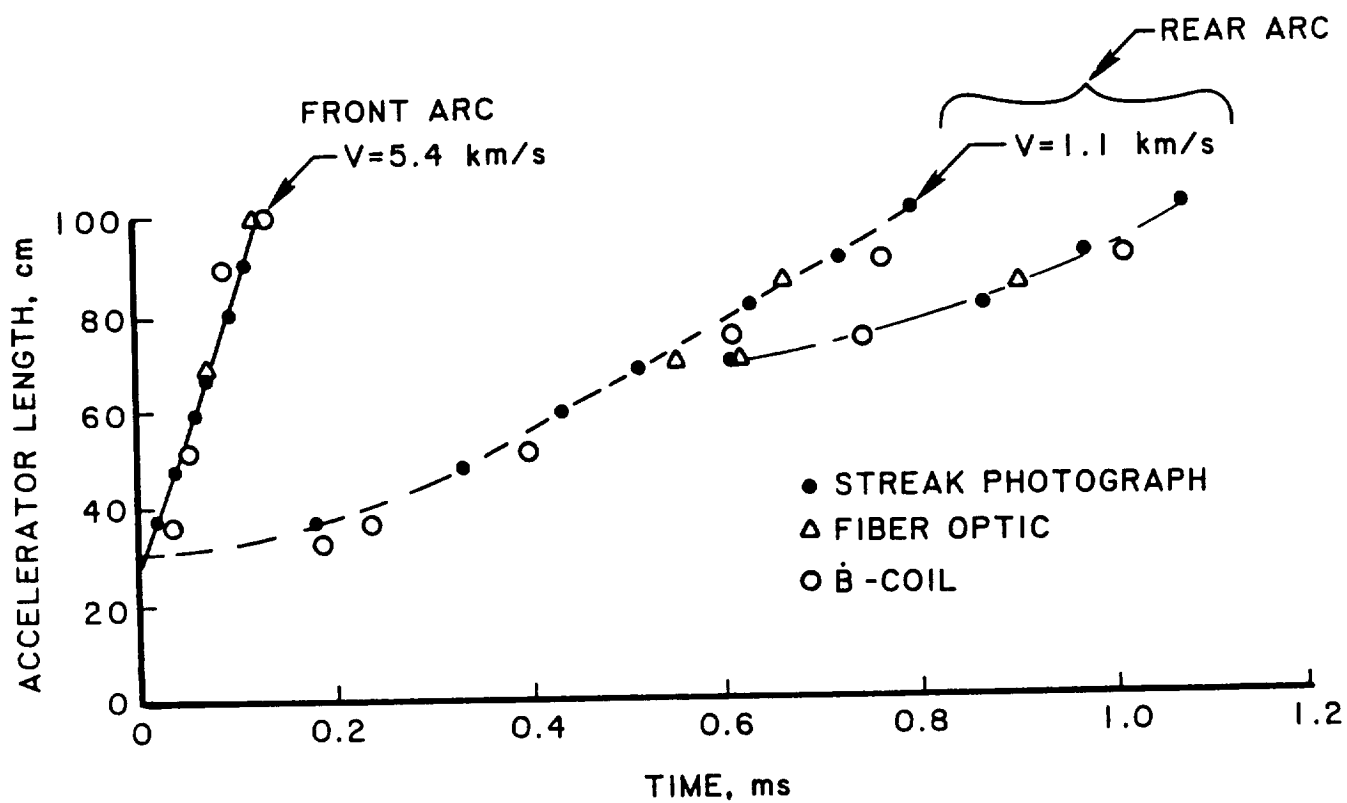
Fig. 17. Position of arcs as a function of time.

REFERENCES

[1] L. M. Zana, W. R. Kerslake, and J. L. Sturman, "Rail accelerators for space transportation," NASA Technical Paper 2571, May, 1986.

[2] J. P. Barber, "Electric rail gun application to space propulsion," AIAA paper no. 79-2091, 1979.

[3] M. N. Kreisler, "How to make things move very fast," American Scientist, 70, 70 (1982).

[4] F. L. Ribe and G. C. Vlases, "Scope of impact fusion and review of macroparticle accelerators," Report LA-8000-C, 1979.

[5] J. F. Kerrisk, "Electrical and thermal modeling of railguns," IEEE Trans. Magns., MAG-20, 399 (1984).

[6] P. K. Ray, "Arc-driven rail gun research," Report NASA CR 174816, December, 1984.

[7] J. V. Parker, W. M. Parsons, C. E. Cummings, and W. E. Fox," Performance loss due to wall ablation in plasma armature railguns," Paper AIAA-85-1575, (1985).

[8] N. M. Schnurr and J. F. Kerrisk, "Numerical studies of ablation and ionization of railgun materials," Paper AIAA-85-1576, (1985).

[9] D. P. Bauer, T. J. McCormick, and J. P. Barber, "Electric rail gun projectile acceleration to high velocity," Paper AIAA-82-1939, (1982).

[10] F. J. Young, H. R. Howland, W. F. Hughes, and D. A. Fikse, "Interactive electromagnetic launcher simulation," IEEE Trans. Magns., MAG-18, 29 (1982).

[11] J. H. Batteh, "Analysis of a rail gun plasma accelerator,"
      Report DAAK11-80-C-0102, Ballistic Research Laboratory,
      December, 1981.

[12] F. F. Chen, Introduction to Plasma Physics. New York:
      Plenum, 1974, pp. 162-165.

[13] I. R. McNab, "Electromagnetic macroparticle acceleration by a
      high pressure plasma," J. Appl. Phys., 51, 2549 (1980).

[14] B. S. Tatenbaum, Plasma Physics. New York: McGraw Hill,
      1967, pp. 347-349.

[15] W. R. Kerslake and B. Z. Cybyk, "Rail accelerator research at
      Lewis Research Center, NASA TM-83015, 1981.

[16] L. M. Zana, W. R. Kerslake, J. C. Sturman, S. Y. Wang, and F.
      F. Terdan, " LeRC rail accelerators: test designs and
      diagnostic techniques," IEEE Trans. Magns., MAG-20, 324
      (1984).

[17] S. Gooder, "Electromagnetic propulsion test facility," NASA
      TM-83568, 1984.

DISTRIBUTION LIST

National Aeronautics and Space Administration
Washington, DC 20546
Attn: RS/Mr. Dell Williams, III   1
       RSE/Mr. Van Landingham   1
       MT/Mr. Ivan Bekey   1

National Aeronautics and Space Administration
Lewis Research Center
21000 Brookpark Road
Cleveland, OH 44135
Attn: Research Support Procurement Section
       Mr. Steve Szabo, MS 501-11   1
       Technology Utilization Office, MS 3-19   1
       Report Control Office, MS 5-5   1
       Library, MS 60-3   2
       Dr. M. Goldstein, Chief Scientist, MS 5-3   1
       Mr. J. Stone, MS 500-219   1
       Mr. D. Byers, MS 500-219   1
       Mr. T. Hardy, MS 500-219   30
       Dr. F. Montegani, MS 3-7   1

National Aeronautics and Space Administration
Lyndon B. Johnson Space Center
Houston, TX 77058
Attn: Mr. Hu Davis   1

National Aeronautics and Space Administration
Marshall Space Flight Center
Huntsville, AL 35812
Attn: Mr. George Von Tiesenhausen, P501   1
       Mr. Robert Bechtel, EB-11   1

Research and Technology Division
Wright-Patterson AFB, OH 45433
Attn: (AFWAL/NASA-PO) Mr. Everett Bailey   1
       (FTD/TQTD) Capt. David G. Hall   1

NASA Scientific and Technical
Information Facility
P.O. Box 8757
Baltimore, MD 21240
Attn: Accessioning Dept.   1

DARPA/TTO
1400 Wilson Boulevard
Arlington, VA 22209
Attn: Dr. Harry D. Fair, Jr.   1

System Planning Corporation
ATM Department
1500 Wilson Boulevard
Arlington, VA 22209
Attn: Dr. Donald E. Shaw   1

ARDC, AMCCOM
Building 382
Dover, NJ 07801
Attn: Dr. Thaddeus Gora   1
       Dr. P. J. Kemmey   1

U.S. Army ARRADCOM
Ballistic Research Lab., DRDAR-BLB
Aberdeen Proving Ground, MD 21005
Attn: Dr. Don Ecceshall   1
       Dr. J. D. Powell   1
       Mr. K. Jamison   1

USAF Rocket Propulsion Laboratory
Edwards AFB, CA 93523
Attn: LKC/Maj. Nordley   1
       LKCJ/Dr. Robert Vondra   1
       LKCS/Mr. Frank Mead   1

USAF Armament Lab (AFATL/DLDB)
Eglin Air Force Base, FL 32542
Attn: Lt. Richard Walley   1

Boeing Aerospace Co.
P.O. Box 3999
Seattle, WA 98124
Attn: Mr. James F. Kenney, MS 8C-23   1

Electromagnetic Launch Research, Inc.
625 Putnam Avenue
Cambridge, MA 02139
Attn: Dr. Henry H. Kolm   1
       Dr. Peter Mongeau   1
       Dr. William Snow   1

GA Technologies
P.O. Box 85608
San Diego, CA 92138
Attn: Dr. Sibley C. Burnett   1
       Dr. Michael M. Holland   1

General Dynamics
P.O. Box 2507
Pamona, CA 91769
Attn: Mr. J. H. Cuadros   1

General Research Corporation
5383 Hollister Avenue
Santa Barbara, CA 93111
Attn: Mr. William M. Isbell   1

GT Devices, Inc.
5705 General Washington Drive
Alexandria, VA 22312
Attn: Dr. Derek Tidman   1
        Dr. Y. C. Thio   1

IAP Research, Inc.
2763 Culver Avenue
Dayton, OH 45429-3273
Attn: Dr. John Barber   1

Physics International Company
2700 Merced Street
San Leandro, CA 94577
Attn: Dr. Ed Goldman   1

LT Aerospace and Defense Company
P.O. Box 225907
Dallas, TX 75265
Attn: Mr. Charles H. Haight   1

Sandia Laboratories
P.O. Box 5800
Albuquerque, NM 87115
Attn: Dr. M. Cowan   1
        Dr. T. J. Burgess   1

Science Applications, Inc.
1503 Johnson Ferry Road
Suite 100
Marietta, GA 30067
Attn: Dr. Jad Batteh   1

Los Alamos National Scientific Laboratory
P.O. Box 1663
Los Alamos, NM 87544
Attn: Dr. J. V. Parker   1
        Dr. Max Fowler   1
        Dr. Will Fox, MS G787   1

Colorado State University
Fort Collins, CO 80521
Attn: Prof. P. J. Wilbur   1
        Prof. H. R. Kaufman   1

Westinghouse Electric Corporation
1310 Beulah Road
Pittsburgh, PA 15235
Attn: Mr. C. J. Mole   1
       Mr. Daniel W. Deis   1

Westinghouse Electric Corporation
401 E. Hendy Avenue
Sunnyvale, CA 94088
Attn: Dr. Ian McNab, MS ED-5   1
       Mr. Ronald A. Rindal, MS ED-2   1

University of Texas at Austin
Center for Electromechanics
Austin, TX 78758
Attn: Dr. John H. Gully   1

University of Texas at Austin
Center for Electromechanics
Austin, TX 78758
Attn: Dr. William E. Weldon   1

Princeton University
Princeton, NJ 08540
Attn: Dean R. G. Jahn   1

Brookhaven National Lab.
Upton, NY 11973
Attn: Dr. James Powell, 802M   1

BDM Corp.
2227 Drake Avenue
Huntsville, AL 35805
Attn: Mr. Steve Mann   1
       Mr. Jim Schaaf   1

BDM Corp.
One 1st National Plaza, Suite 1010
Dayton, OH 45402
Attn: Mr. Keith J. Maxwell   1

Austin Research Assoc.
1901 Rutland Drive
Austin, TX 78758
Attn: Dr. William E. Drummond   1

General Electric Co.
ARD No. 3, Plains Road
Ballston Spa, NY 12020
Attn: Mr. Wendell Neugebaur   1

Auburn University
Attn: Dr. Anthony K. Hyder
       202 Samford Hall
       Auburn, AL 36849   1

Auburn University
Attn: Dr. M. F. Rose
       Director, Space Power Institute
       Auburn, AL 36849   1

1. Report No. NASA CR 179584	2. Government Accession No.	3. Recipient's Catalog No.
4. Title and Subtitle Arc-Driven Rail Accelerator Research		5. Report Date February, 1987
		6. Performing Organization Code
7. Author(s) Pradosh K. Ray		8. Performing Organization Report No.
		10. Work Unit No. YOS 2415 RTOP 506-55-22
9. Performing Organization Name and Address Mechanical Engineering Department Tuskegee University Tuskegee, AL 36088		11. Contract or Grant No. NAG 3-76
12. Sponsoring Agency Name and Address NASA Lewis Research Center 21000 Brookpark Rd. Cleveland, Ohio 44135		13. Type of Report and Period Covered Final Report
		14. Sponsoring Agency Code LeRC Code 5323

15. Supplementary Notes

16. Abstract

The experiment of Bauer et al. [9] is analyzed by considering wall ablation and viscous drag in the plasma. Plasma characteristics are evaluated through a simple fluid-mechanical analysis considering only wall ablation. By equating the energy dissipated in the plasma with the radiation heat loss, the average properties of the plasma are determined as a function of time and rate of ablation.

Locations of two simultaneously accelerating arcs were determined by optical and magnetic probes and from streak camera photographs. All three measurements provide consistent results.

17. Key Words (Suggested by Author(s)) Rail Accelerator High-Velocity Projectile Plasma Acceleration Arc Diagnostics		18. Distribution Statement Unclassified--Unlimited	
19. Security Classif. (of this report) Unclassified	20. Security Classif. (of this page) Unclassified	21. No. of pages 46	22. Price*